Semiclassical theory of alignment effects in near-resonant energy-transfer collisions of rare-gas atoms with aligned Rydberg atoms

Eric G. Layton
Joint Institute for Laboratory Astrophysics, University of Colorado, Boulder, Colorado 80302

Michael A. Morrison*
Department of Physics and Astronomy, University of Oklahoma, Norman, Oklahoma 73019-0225

(Received 29 September 1999; published 17 April 2001)

Recent experiments [E. M. Spain *et al.*, J. Chem. Phys **102**, 24 (1995)] discovered alignment effects in cross sections for near-resonant energy-transfer collisions of Xe atoms with Ca Rydberg atoms at a single mean relative velocity. A collaborative quantum-mechanical study [W. Isaacs and M. A. Morrison, Phys. Rev. A **57**, R9 (1998)] confirmed these findings and discovered pronounced oscillations in the velocity dependence of state-to-state cross sections. Collisions corresponding to the $17d_{m_0} \rightarrow 18p_m$ transitions in the Ca-He system are here analyzed semiclassically. This analysis shows that the origin of these oscillations is a phase interference process unique to Rydberg target states. We further demonstrate the importance of retaining the energy defect and of using quantum-defect phase-shifted radial functions in calculations of alignment cross sections for Rydberg states.

DOI: 10.1103/PhysRevA.63.052711 PACS number(s): 34.60.+z

I. INTRODUCTION

In conventional low-energy electron-atom scattering experiments, with the target gas in a cell or beam, atoms in an initial state $n_0 l_0$ are uniformly distributed among magnetic sublevels $m_0 = -l_0, \ldots, +l_0$. These experiments determine averages over initial and sums over final sublevels, such as the level-to-level integral cross section

$$\sigma_{n_0 l_0 \rightarrow nl} = \frac{1}{2l_0+1} \sum_{m_0=-l_0}^{l_0} \sum_{m=-l}^{l} \sigma_{n_0 l_0 m_0 \rightarrow nlm}. \qquad (1)$$

Such experiments yield no information about the role of the magnetic quantum number m in the scattering process. One cannot determine, for example, whether energy transfer in one ''m channel'' ($m_0 \rightarrow m$) is more or less efficient than another. Nor can one ascertain whether the interaction preserves or obliterates information about the initial distribution of target states among magnetic sublevels. Such insights require an initial state with an *anisotropic* distribution of magnetic sublevels. With the advent of pulsed lasers, the preparation of such states became feasible, and studies of collisions involving laser-excited initial states of atoms began to proliferate [1–11]. Alignment phenomena have generated great interest because of the detailed insight they provide into fundamental mechanisms that influence the dynamics and properties of colliding particles [12–16].

Two types of nonstatistical distributions can be realized: an *aligned state*, in which the probability $p(m_0)$ of finding an atom in sublevel m_0 depends on the magnitude but not on the sign of m_0, i.e., $p(-m_0) = p(+m_0)$, and an *oriented state*, in which the population depends on both the magnitude and sign of m_0, i.e., $p(-m_0) \neq p(+m_0)$ (see, for example, Ref. [17] and references therein). Here the magnetic quantum numbers refer to a quantization axis chosen parallel to the relative velocity of the projectile and target, i.e., the collision axis. In this paper, we are concerned with collisions involving aligned states, which can be prepared via absorption induced by linearly polarized lasers [8,10].

Nearly all experiments on collisions of projectile atoms with aligned target atoms prepare the target in a *low-lying excited state*. Prototypical are the experiments by Leone and collaborators on spin changing and fine-structure changing near-resonant energy-transfer collisions of calcium with various nonreactive rare-gas atoms [1–11]. In these experiments, one, two, or three linearly polarized lasers are used to excite Ca to low-lying aligned p, d, or f excited states, respectively; for d and f states, the relative orientation of the electric field vectors of the lasers can be adjusted to produce initial states with quite different spatial distributions of electron density. Alignment curves are obtained by varying the angle β between the relative velocity $\mathbf{v}$ and the electric field $\mathbf{E}_L$ of one of the lasers. The variations of these cross sections with β signify alignment effects; the intensity of these variations quantifies the strength of these effects. Experimentally, varying β changes the admixture of magnetic substates in the initial state, altering the ''shape'' of the electron probability density. Alignment phenomenon signal that, in effect, the target ''remembers'' its initial alignment characteristics through the collision. In addition to demonstrating such phenomena, data from these experiments has revealed the relative efficiency of various pathways for energy transfer, distinguished by the magnitude of the initial magnetic quantum number [4,6].

These data have been interpreted in terms of ''orbital locking and following'' models, which are predicated on the formation during the collision of a transient quasimolecular electronic state [2,18,19]. In this picture the orbital of the excited electron temporarily couples to the internuclear axis

*Electronic address: morrison@mail.nhn.ou.edu; www.nhn.ou.edu/~morrison

of the quasimolecule within a few tens of bohr of the coordinate origin. Consequently, depending on the distance at which the orbital ''locks'' and on the symmetry of the resulting electronic state, cross sections may exhibit alignment effects of varying degree. Theoretically, avoided crossings of relevant potential-energy curves are invoked to determine which symmetry of the quasimolecular state is primarily responsible for energy transfer. Except for the work of Hickman on Ca–Xe collisions [20,21], applications of this model have been rendered qualitative by the lack of accurate potential-energy curves for systems of interest. Nevertheless, analyses in terms of ''orbital locking and following'' theory have added significantly to our understanding of the dynamics of energy transfer [12,13].

A quite different physical situation occurs if the initial state of the target atom is a Rydberg state. In this case, the electron's extremely diffuse probability density and the high-energy density of accessible bound states make problematic a molecular (Born–Oppenheimer) description of the dynamics [22,23]. Indeed, orbital locking theories predict that no alignment effects will appear if the initial aligned state is highly excited, for molecular bond formation is not an important collision mechanism. To explore this new physical realm, a joint experimental-theoretical investigation was initiated, with measurements of alignment effects in thermal state-changing collisions involving aligned Ca Rydberg atoms and rare-gas atoms by Leone and collaborators [24,25] and a dual theoretical program consisting of complementary quantum [26,27] and semiclassical calculations.

The experimental and quantum-mechanical components of this project recently reported the unexpected presence of pronounced alignment effects in cross sections for near-resonant energy-transfer collisions of Xe with Rydberg Ca atoms. Measurements by Spain *et al.* [25] revealed unambiguous alignment effects in cross sections for the $17d \rightarrow 18p$ at a single mean relative velocity; e.g., a marked preference for end-on encounters when the Ca atom is prepared in a d_{z^2} state.

Quantum calculations by Isaacs and Morrison [26,27] confirmed these results and, by exploring a wide range of relative velocities, uncovered oscillatory structures in cross sections for this and other transitions in both Ca–Xe and Ca–He collisions. *The theoretical formulation used in the quantal calculations explicitly precluded the formation of a quasimolecular state*. So the origin of the alignment effects, the oscillations, and their dependence on the initial and final magnetic quantum numbers of the electron remained a mystery.

In the present paper we seek to resolve these mysteries by analyzing alignment effects in near-resonant Ca–He collisions using the semiclassical impact parameter method. (A preliminary account of this paper has appeared in Ref. [28].) Our theoretical formulation allows easy identification of aspects of the system that are crucial to the observed features (e.g., the role of the energy defect and the phase shift in the electron's radial functions due to quantum defects). Moreover it leads to an explanation of the aforementioned oscillations as due to an interference process unique to Rydberg target states. It explains the disappearance of these oscillations at large relative velocities (greater than a few thousand meters per second). Finally, it elucidates the striking dependence of these oscillations on the initial and final magnetic quantum numbers.

Section II summarizes key properties of alignment phenomena and defines relevant quantities. Our theoretical formulation is described in Sec. III. Although the emphasis in this paper is on the Ca–He cross sections in Sec. IV B, we first present results for l mixing in Na–He collisions: in Sec. IV A we use this well-studied problem [29–32] to test our formalism, its underlying approximations, and our numerical application. In Sec. IV we also show that two approximations widely used in previous studies of conventional rare-gas atom—Rydberg atom collisions—neglect of the energy defect and use of hydrogenic wave functions—produce serious errors in alignment studies. Finally, Sec. V offers our interpretation of the oscillations under discussion.

II. ALIGNMENT EFFECTS

The preparation of an initially aligned state by a linearly polarized laser introduces into the dynamics the direction of the electric field $\mathbf{E}_L$. (If more than one laser is used, e.g., to prepare an aligned d state, then $\mathbf{E}_L$ is usually chosen as the electric field of the first laser.) The subsequent collision defines a second direction, the initial relative velocity $\mathbf{v}$, which is an axis of rotational symmetry for the collision. This vector further defines the z axis of the collision frame. The *alignment-selected cross sections* $\sigma_{n_0 l_0 \rightarrow nl}(\beta;v)$ that are measured in the ''two-vector correlation experiments'' of Leone and collaborators are near-resonant energy-transfer cross sections for the transition $n_0 l_0 \rightarrow nl$ as a function of the angle β between $\mathbf{v}$ and $\mathbf{E}_L$. A least-squares fit to these data yields magnetic sublevel cross sections $\sigma^{|m_0|}(v)$. This cross section is the sum over all final magnetic sublevels of the state-to-state cross sections,

$$\sigma^{|m_0|}(v) = \sum_{m=-l}^{l} \sigma_{n_0 l_0 m_0 \rightarrow nlm}(v). \tag{2}$$

One such cross section is obtained for each initial magnetic quantum number m_0.

The fundamental theoretical quantities for describing these collisions are the scattering amplitudes $f(\mathbf{K},nlm \leftarrow \mathbf{K}_0, n_0 l_0 m_0)$ for initial and final relative momenta $\mathbf{K}_0$ and $\mathbf{K}$ and for all allowed initial and final magnetic substates m_0 and m. In the collision frame, with the z axis coincident with the initial relative velocity, $\hat{\mathbf{K}} = (\theta,\varphi)$ are the scattering angles. From these amplitudes (or from the scattering matrix in the collision frame) one can compute the magnetic sublevel cross sections $\sigma^{|m_0|}(v)$.

These cross sections are independent of the sign of m_0 because of reflection symmetry in the scattering plane formed by $\mathbf{K}_0$ and $\mathbf{K}$. They are related to alignment-selected cross sections by the diagonal elements of the density matrix for the initial state,

$$\sigma_{n_0 l_0 \to nl}(\beta;v) = \sum_{m_0=-l_0}^{l_0} \rho^{(l_0)}_{m_0,m_0}(\beta)\sigma^{|m_0|}(v). \qquad (3)$$

The density-matrix element $\rho^{(l_0)}_{m_0,m_0}(\beta)$, appropriately normalized [17], is the probability for finding the Rydberg electron in a state with quantum numbers l_0 and m_0. For a pure state, this element is given by the reduced Wigner matrix element, $p(|m_0|)=\rho^{(l_0)}_{m_0,m_0}(\beta)=d^{(l_0)}_{m,m_0}(\beta)$. Equation (3) effectively deconstructs the alignment cross section into ''kinematic quantities'' $\rho^{(l_0)}_{m_0,m_0}(\beta)$, which fully account for the alignment properties of the particular initial state, and ''dynamical quantities,'' the magnetic sublevel cross sections $\sigma^{|m_0|}$. Absent alignment effects, the latter cross sections are independent of $|m_0|$, and the sum in Eq. (3) is independent of β. *So the extent to which each cross section $\sigma^{|m_0|}(v)$ depends on $|m_0|$ at a particular relative velocity v is a measure of the strength of the alignment effect at that velocity; if these cross sections are independent of $|m_0|$, then no such effects are present and the collision has obliterated all information concerning the initial alignment of the Rydberg electron* [9]. Thus the magnetic sublevel cross sections fully describe alignment phenomena; they are the data we present in Sec. IV B.

III. THEORY OF STATE-TO-STATE CROSS SECTIONS

To calculate either l-mixing or magnetic sublevel cross sections we require amplitudes for the state-to-state transitions $\alpha_0=(n_0\,l_0\,m_0)\to\alpha=(nlm)$ for all magnetic quantum numbers m_0 and m allowed by the orbital angular momenta l_0 and l of the excitation $(n_0\,l_0)\to(nl)$. As our theoretical treatment is the same for both types of cross sections, we here describe this common methodology, leaving details of particular scattering quantities to the relevant subsections in Sec. IV.

Figure 1 shows the geometry of the collision and relevant variables. The collision frame is defined by its origin—the nucleus of the Ca^+ core—and its z axis (with unit vector $\mathbf{e}_z$), which is parallel to the initial relative velocity $\mathbf{v}$. We adopt the ''quasifree-electron model'' [22,33,34] in which the core functions as a ''spectator,'' a point particle that does not participate in the collision. Rather, its role is to support the initial and final states of the Rydberg electron. In the collision frame, then, the relative velocity reduces to the projectile velocity. The system wave function depends on the spatial variables $\mathbf{r}$ of the Rydberg electron and on those of the rare-gas projectile $\mathbf{R}$. In the semiclassical approximation, however, the latter variables are treated classically as $\mathbf{R}=\mathbf{R}(t)$. So the system wave function reduces to the Rydberg electron wave function and thus depends only on $\mathbf{r}$. The evolution of the system is described by a set of coupled Schrödinger–Hamilton equations.

For the collisions considered here, the inelasticity is very small compared to the relative kinetic energy. So the classical trajectory of relative motion should be quite undisturbed and well approximated as rectilinear [35,36]. Identifying b as the impact parameter of the projectile, we write

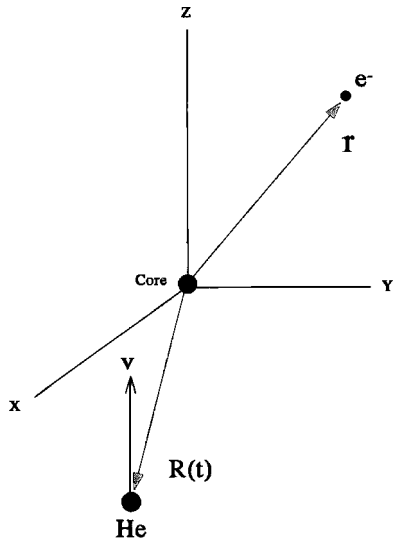

FIG. 1. Geometry and coordinates for semiclassical description of collisions of a rare-gas atom by a Rydberg electron in the collision frame.

$$\mathbf{R}(t)=b\mathbf{e}_x+vt\mathbf{e}_z, \qquad (4)$$

where we have exploited the axial symmetry of the collision to choose a trajectory that intersects the x axis (with unit vector $\mathbf{e}_x$) at b. We describe the interaction of the rare-gas projectile with the Rydberg electron as a binary encounter represented by a point contact potential discussed below. We describe the quantum states of the Rydberg electron as stationary angular momentum eigenstates labeled by quantum numbers n, l, and m. Within this model we calculate final-state transitions amplitudes numerically using first-order time-dependent perturbation theory [37–40].

The semiclassical impact parameter method has a long, successful history in research on atomic collisions in general [35] and Rydberg atom-rare-gas collisions in particular [20,23]. Of particular relevance to the present study is the semiclassical analysis of inelastic n, l changing and quasielastic l-mixing collisions of rare-gas projectiles with Rydberg-atom targets by Lebedev and Fabrikant [36] (see also Sec. 4.3 and 6.3 of Ref. [41] and references therein). These authors combined the impact-parameter method with normalized perturbation theory to derive elegant analytic expressions and simple scaling formulas for the probabilities and cross sections for such collisions.

Treating the relative motion of the rare-gas projectile and the atomic core classically is a good approximation provided the de Broglie wavelength associated with this motion is small compare to the size of the target atom [42]. This requirement is easily met for collisions of interest here; the radius of the Rydberg atom is huge, and the projectile-core system has a large reduced mass and thus a small de Broglie wavelength.

In our investigations the projectile is helium. Because the first excitation threshold of He ($\approx$20 eV) is well above the binding energies of the Rydberg electron, and the polarizability of He (0.2501 $Å^3$) is small [43], we treat this projectile as a structureless point mass. Since the Rydberg electron

is distributed over a large volume of space and its probability density is correspondingly small, the electron–He interaction is weak and acutely nonadiabatic, consisting primarily of an impulse from the projectile to the electron. We model this interaction using the Fermi contact potential

$$\hat{V}(t)=2\pi A\left(\frac{\hbar^2}{m_e}\right)\delta(\mathbf{r}-\mathbf{R}), \tag{5}$$

where $A=1.19a_0$ is the electron-He scattering length [44,45]. Originally introduced by Fermi in studies of pressure shifts in the spectra of alkali Rydberg atoms perturbed by rare buffer gases [33], this model has been widely used in subsequent research on Rydberg atom-rare-gas collisions [20,23]. For rare-gas perturbers heavier than helium, effects arising from the perturbation of the projectile's ground-state electron density by the Rydberg target electron become important. Lebedev and Fabrikant [36] have shown how to modify the simple scattering length approximation used here, according to which the electron-rare-gas scattering amplitude equals $-A$, to accommodate these effects.

We expand the semiclassical wave function of the Rydberg electron in a basis of bound states as

$$\Psi(\mathbf{r},t)=\sum_{\alpha} a_{\alpha}(t)\psi_{\alpha}(\mathbf{r})e^{-i\epsilon_{nl}t/\hbar}, \tag{6}$$

where $a_{\alpha}(t)$ is a transition amplitude and ϵ_{nl} is the quantum-defect shifted energy in atomic units (hartree)

$$\epsilon_{nl}=-\frac{1}{2(n-\delta_{nl})^2}. \tag{7}$$

For the Rydberg states of Ca considered here, the quantum defects δ_{nl} are $\delta_{17d}=0.9043$ and $\delta_{18p}=1.8721$. For collisions with Rydberg atoms, this expansion is more appropriate than one in quasimolecular states, which yields a complicated set of coupled equations and requires accurate potential-energy curves. For collisions in which the target atom is not in a Rydberg state, however, an expansion in quasimolecular states would be suitable [46,47]; in such a collision the target is more ''opaque,'' i.e., its interaction with the projectile is stronger, in part due to increased target electron density.

Neglecting spin-orbit and spin-spin interactions renders the Rydberg atom core spherically symmetric, and we can write its Hamiltonian eigenfunctions in terms of radial functions $u_{nl}(r)$ as

$$\psi_{\alpha}(\mathbf{r})=\frac{1}{r}u_{nl}(r)Y_{lm}(\theta,\varphi). \tag{8a}$$

Here $Y_{lm}(\theta,\varphi)$ is a spherical harmonic [48] whose axis of quantization is the z axis of the collision frame

$$Y_{lm}(\theta,\varphi)=N_{lm}P_l^{|m|}(\cos\theta)e^{im\varphi}, \tag{8b}$$

with normalization constant

$$N_{lm}=(-1)^m\sqrt{\frac{(2l+1)}{4\pi}\frac{(l-m)!}{(l+m)!}}. \tag{9}$$

The radial function can either be approximated analytically as hydrogenic [48], calculated in the JWKB approximation [36], or computed numerically in the Coulomb approximation [49,50]. The latter approach, used here and described below, introduces a phase shift in each radial function from its pure hydrogenic form, the amount of the shift being the quantum defect for the state. This approach thus incorporates (semiempirically) the effects of the core electrons on the initial and final states of the Rydberg electron—inclusion of which is essential to alignment phenomena [see Sec. IV B].

The evolution of the system is described by the Schrödinger equation

$$i\hbar\frac{\partial}{\partial t}\Psi(\mathbf{r},t)=\hat{\mathcal{H}}(t)\Psi(\mathbf{r},t) \tag{10}$$

and the rectilinear trajectory $\mathbf{R}(t)$ of Eq. (4). The Hamiltonian $\hat{\mathcal{H}}(t)$ is the sum of the Rydberg electron Hamiltonian and the Fermi potential (5). Upon inserting the expansion (6) into Eq. (10), we obtain the usual initial value problem

$$\frac{d}{dt}a_{\alpha}(t)=-\frac{i}{\hbar}\sum_{\alpha'} a_{\alpha'}(t)e^{i\Delta\epsilon t/\hbar}\langle\psi_{\alpha}|\hat{V}(t)|\psi_{\alpha'}\rangle, \tag{11}$$

where we note that the transition amplitudes $a_{\alpha}(t)$ are intrinsically collision frame quantities. The energy defect $\Delta\epsilon \equiv \epsilon_{n',l'}-\epsilon_{nl}$ embodies the inelasticity of the transition. Using the Fermi potential (5) to evaluate the coupling matrix elements transforms these equations to

$$\frac{d}{dt}a_{\alpha}(t)=-2\pi iA\left(\frac{\hbar}{m}\right)\sum_{\alpha'} a_{\alpha'}(t)e^{i\Delta\epsilon t/\hbar}\mathcal{P}_{\alpha'\alpha}[\mathbf{R}(t)], \tag{12}$$

where we have introduced the *transition density*

$$\mathcal{P}_{\alpha'\alpha}(\mathbf{r})\equiv\psi^*_{\alpha'}(\mathbf{r})\psi_{\alpha}(\mathbf{r}) \tag{13}$$

evaluated at $\mathbf{r}=\mathbf{R}(t)$. The variation of the transition amplitudes $a_{\alpha}(t)$ with time quantifies the effect on the Rydberg electron of the passage of the He atom through regions of varying initial- and final-state electron density. This interpretation becomes key to understanding the oscillations in the resulting cross sections, as discussed in Sec. IV B. State-to-state cross sections are calculated from these amplitudes in the $t\rightarrow\infty$ limit.

The principal maximum of the Rydberg electron radial function increases with n roughly as n^2. The resulting highly diffuse electron density in the initial and final states suggests evaluating the transition amplitudes via time-dependent perturbation theory. To first order, the solutions of Eq. (12) are

$$a_\alpha(t\to+\infty)=a_\alpha(t\to-\infty)-i(2\pi A)\left(\frac{\hbar}{m_e}\right)\times\sum_{\alpha'}\ a_{\alpha'}(t\to-\infty)\int_{-\infty}^{\infty}e^{i\Delta\epsilon t/\hbar}\mathcal{P}_{\alpha'\alpha}[\mathbf{R}(t)]dt. \tag{14}$$

To evaluate these amplitudes, we change the variable of integration from t to z. Using cylindrical coordinates $[b,\varphi,z(t)]$, with $z(t)=vt$, and introducing the radial function via Eq. (8a) and the associated Legendre polynomial $P_l^{|m|}(\cos\theta)$ in the spherical harmonic (8b), we obtain the explicit form

$$a_\alpha(t\to+\infty)=a_\alpha(t\to-\infty)-i\frac{4\pi A}{v}\left(\frac{\hbar}{m_e}\right)\times\sum_{\alpha'}\ a_{\alpha'}(t\to-\infty)N_{lm}N_{n'l}e^{i(m'-m)\phi}\times\int_0^{\infty}P_l^{|m|}\left(\frac{z}{R}\right)P_l^{|m'|}\left(\frac{z}{R}\right)u_{nl}(R)\times u_{n'l'}(R)J(z;v,\Delta\epsilon)dz, \tag{15}$$

where $R^2=z^2+b^2$. The function

$$J(z;v,\Delta\epsilon)\equiv\left\{\begin{matrix}\cos\\ \sin\end{matrix}\right\}\left(\frac{\Delta\epsilon}{\hbar v}z\right)\quad\text{for}\ \ l+l'+|m|+|m'|\left\{\begin{matrix}\text{even}\\ \text{odd}\end{matrix}\right. \tag{16}$$

embodies the symmetry under inversion of the transition amplitudes.

We evaluate the integral in Eq. (15) using an adaptive Simpson's rule algorithm. The maximum value of z is determined from the radius that contains 0.9999 of the electron probability. To determine our error tolerance we checked known quantities such as hydrogenic radial expectation values.

We then obtain state-to-state cross sections by integrating the transition probability

$$P_{\alpha_0\to\alpha}(v;b)=|a_\alpha(t\to+\infty)|^2 \tag{17}$$

over the unobserved variables b and φ:

$$\sigma_{\alpha_0\to\alpha}(v)=2\pi\int_0^{\infty}P_{\alpha_0\to\alpha}(v;b)b\,db. \tag{18}$$

We also evaluate this integral using Simpson's rule, finding that a step size in impact parameter of $\Delta b=0.1a_0$ gives excellent convergence.

For purposes of interpretation, it is useful to write the transition probability (17) in terms of the transition density (13) expressed in cylindrical coordinates:

$$P_{\alpha_0\to\alpha}(v;b)=\left(\frac{2\pi A\hbar}{m_e}\right)^2\frac{1}{v^2}\int_{-\infty}^{\infty}\int_{-\infty}^{\infty}\exp i\Delta\epsilon(z-z')/(\hbar v)\times\mathcal{P}_{\alpha,\alpha_0}(z,b)\mathcal{P}_{\alpha,\alpha_0}(z',b)dz\,dz', \tag{19a}$$

we have used the fact that the transition density (13) is real and independent of the azimuthal angle φ. The sine functions in the phase of the integrand average to zero upon integration over z and z', leaving

$$P_{\alpha_0\to\alpha}(v;b)=\left(\frac{4\pi A\hbar}{m_e}\right)^2\frac{1}{v^2}\int_0^{\infty}\int_0^{\infty}\cos\left[\frac{\Delta\epsilon}{\hbar v}(z-z')\right]\times\mathcal{P}_{\alpha,\alpha_0}(z,b)\mathcal{P}_{\alpha,\alpha_0}(z',b)dz\,dz', \tag{19b}$$

where we have invoked the symmetry of the transition density with respect to the *xy* plane of the collision frame. Note that in the integrand, the argument of the cosine contains the only dependence on the relative velocity and the energy defect $\Delta\epsilon$, and the transition densities contain the only dependence on the initial and final magnetic quantum numbers.

In practice, evaluation of the state-to-state cross sections is made much more efficient by writing the transition probability Eq. (19b) in terms of Fourier transforms of the transition density, namely,

$$P_{\alpha_0\to\alpha}(v;b)=4\left(\frac{2\pi A\hbar}{m_e}\right)^2\frac{1}{v^2}[\mathcal{F}_{\alpha'\alpha}(v;b)]^2, \tag{20a}$$

where $\mathcal{F}_{\alpha'\alpha}(v;b)$ is the Fourier sine or cosine transform

$$\mathcal{F}_{\alpha'\alpha}(v;b)=\int_0^{\infty}\left\{\begin{matrix}\sin\\ \cos\end{matrix}\right\}\left(\frac{\Delta\epsilon}{\hbar v}z\right)\mathcal{P}_{\alpha'\alpha}(z,b)dz\quad\text{for}\ \ l+l'+|m|+|m'|\left\{\begin{matrix}\text{even}\\ \text{odd}\end{matrix}\right. \tag{20b}$$

This step reduces evaluating the transition probability to a single integral over the rare-gas trajectory and shows that this quantity is positive definite.

The above expressions for the state-to-state transition probability and for the corresponding cross section assume that only one l manifold is populated in a pure state. Similar formulas will result if two or more l manifolds are populated incoherently. But if these manifolds are in a coherent superposition, then our expressions must be modified to allow for interference.

To conclude this section, we note two important differences between this formulation and those of prior applications of the semiclassical impact parameter method to Rydberg atom-rare gas collisions. In their studies of l mixing in sodium Rydberg atoms, Gersten [37] and Derouard and Lombardi [39] assumed that the energy defect $\Delta\epsilon$ was negligible. Equation (14) shows that this assumption yields a larger cross section than if the defect is included properly. For l-mixing cross sections in Na neglect of the energy defect is not serious (see Sec. IV A). But $\Delta\epsilon$ must not be set to zero in calculations of magnetic sublevel cross sections for alignment studies (see also Ref. [36]). As we shall demon-

strate in Sec. IV B, the energy defect plays a crucial role in explaining the oscillatory behavior of magnetic sublevel cross sections. This point is evident from Eq. (19b); in the limit that the argument of the exponential vanishes, the transition probability and therefore the state-to-state cross section exhibit a simple inverse square dependence on velocity.

The second difference concerns our choice of the axis of spatial quantization. Using the z axis, as in the collision frame adopted here, yields symmetry properties that provide insight and simplify cross section calculations. For example, in the limit where $\Delta\epsilon/v \to 0$, only transitions for which $l + m + l' + m'$ is even (or zero) are allowed. Although this approximate symmetry is broken when the limit is not attained, it does explain the high-energy behavior of the state-to-state cross sections calculated using the quantum-mechanical impulse approximation [26,27].

Third, many prior studies of Rydberg-atom rare-gas scattering approximate the radial function $u_{nl}(r)$ by those of atomic hydrogen in the pure-Coulomb approximation. For rare-gas collisions with aligned Rydberg atoms, this approximation grossly underestimates state-to-state cross sections and misrepresents the alignment effects (see Sec. IV B). To some extent, this failure results from the comparatively large quantum defects for the states of Ca of interest. The hydrogenic approximation is adequate for studies of l mixing in sodium.

IV. RESULTS AND DISCUSSION

We begin in Sec. IV A with l-mixing collisions of He with Na Rydberg atoms. We do so to validate our model, to verify our numerical procedures and codes, and to explore values of the principal quantum number n of the Rydberg electron at which the binary encounter mechanism is valid. We then turn to alignment phenomena in Ca–He collisions in Sec. IV B.

A. Angular momentum mixing processes

Gallagher and co-workers [51–55] performed a series of experiments in which rare buffer gases were introduced into a cell of alkali atoms in an excited configuration $n_0 l_0$ at absolute temperature T. They observed a lengthening of the lifetime of the excited atoms, which they attributed to collision-induced transitions to configurations with same n_0 but different l_0. Studying the process

$$\mathrm{Na}(n_0 d) + \mathrm{He} \to \mathrm{Na}(n_0 l) + \mathrm{He} \quad (l > 2) \tag{21}$$

for values of n_0 from 5 to 15, they found that for $n_0 \leqslant 10$, the l-mixing cross section $\sigma^{(l\ \mathrm{mix})}_{n_0,l_0}(v)$ increases with n_0 as n_0^4, while beyond $n_0 = 10$ this cross section declines.

The l-mixing cross section is just the sum over $l > l_0$ of the level-to-level cross sections of Eq. (1),

$$\sigma^{(l\ \mathrm{mix})}_{n_0,l_0}(v) = \sum_{l>l_0} \sigma_{n_0 l_0 \to n_0 l}(v). \tag{22}$$

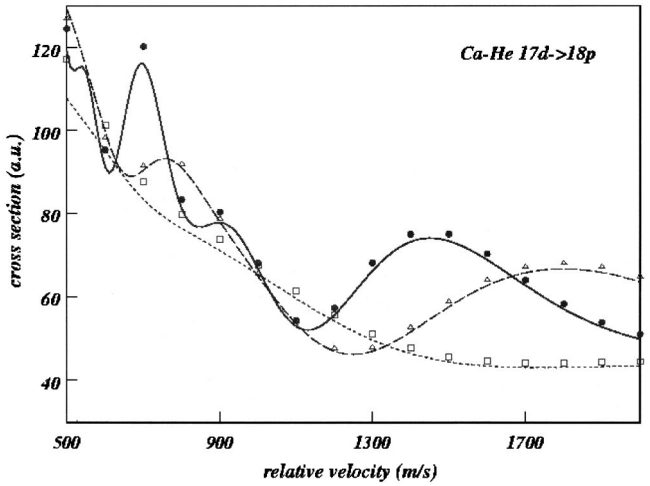

FIG. 2. Partial magnetic cross sections for $17d \to 18p$ transitions in Ca–He collisions. The present semiclassical results (points) are compared to the quantum mechanical cross sections of Isaacs and Morrison [27] (lines) for $|m_0| = 0$ (solid line and closed circles), 1 (long dash line and open triangles), and 2 (short dash line and open squares).

To compare with measured data, this cross section must be averaged over the Maxwell–Boltzmann distribution of relative velocities appropriate to the gas temperature T,

$$\overline{\sigma}^{(l\ \mathrm{mix})}_{n_0,l_0}(v) = \frac{\langle \sigma^{(l\ \mathrm{mix})}_{n_0,l_0}(v) v \rangle}{\langle v \rangle} \approx \frac{\mu v^2}{2k_B T} \sigma^{(l\ \mathrm{mix})}_{n_0,l_0}(v), \tag{23}$$

where μ is the reduced mass ($3.409u$ for Na-He) and k_B is Boltzmann's constant. Here we have adopted the approximate form of Derouard and Lombardi [39]. The conditions for validity of this form are well-satisfied for the process (21) because the quantum defects for $l > 1$ states of Na are small [56]. Note, however, that unlike Derouard and Lomarbdi, who were primarily interested in more highly excited states for which $\Delta\epsilon$ is quite small, we do not set the energy defect to zero.

Several theoretical papers have addressed this phenomenon [29,31,36,37,39,40,57–59]. Gersten [37], using a model based on the semiclassical impact parameter method with a quasifree-electron interaction between the rare-gas and the Na target, reported results for $n_0 = 4-7$. Gersten neglected the energy defects and, because the assumptions of his model are invalid at small atomic radii for $n_0 \leqslant 10$, used a hard collision approximation for projectile impact parameters less than a critical value b_0. In semiclassical time-dependent perturbation theory, the contribution to the integral in Eq. (18) over impact parameter b from small impact parameters tends to overestimate the transition probability. However, the agreement in Fig. 2 between quantal and semiclassical cross sections at all but the lowest relative velocities suggests that in the present application this effect may be negligible except at these low velocities. Gersten [37] proposed correcting for this overestimation, a consequence of the increased coupling at small impact parameter between the initial and final target Rydberg states, by setting the tran-

TABLE I. Cross sections for l mixing in units of 1000 Å^2.

Level	Theory[a]	Theory (present)	Experiment[b]
6D		8.94	0.38(7)
9D	5.15	4.42	1.04(20)
10D	3.93	3.51	2.2(8)
11D	3.00	2.80	1.85(20)
12D	2.37	2.25	1.69(30)
13D	1.93	1.84	1.65(30)
14D	1.59	1.51	1.33(20)

[a]Deouard and Lombardi [39].
[b]Gallagher *et al.* [51,53].

sition probability at some value b_0 equal to an arbitrary constant; Lebedev and Fabrikant [36] have discussed this stratagem and applied it to studies of heavy-rare-gas atom collisions with Rydberg Rb atoms (see also Sec. 6.2 of Ref. [41]). Because the choice of this constant is ambiguous and because the comparison in Fig. 2 show that the existence and characteristics of the oscillations in the present state-to-state cross sections do not hinge on this point, we have not implemented this correction.

Derouard and Lombardi [39] followed a methodology similar to Gersten but did not invoke the hard collision approximation. Because they neglect energy defects, their cross sections depend inversely on the square of v. Their velocity averaged l-mixing cross sections with $n_0=8-14$ began to agree with experiment at about $n_0=10$. They also were able to fit their cross sections to an n_0^4 dependence, consistent with experimental findings.

Table I compares our velocity-averaged l-mixing cross sections with those of Derouard and Lombardi and with the experimental data of Gallagher *et al.* All results correspond to $T=430$ K. Unlike the data, neither theoretical result shows an initial increase with n_0. Our cross sections, which include the energy defect, are smaller than those of Derouard and Lombardi, who set $\Delta\epsilon$ to zero. The effect of this approximation on $\bar{\sigma}^{(l\ \mathrm{mix})}_{n_0,l_0}(v)$ is far less important than on the Ca-He alignment cross sections of Sec. IV B. [For purposes of direct comparison, we also computed l-mixing cross sections in the zero-defect approximation. For 10D and 11D, respectively, we found the values (in units of 1000 Å^2) 3.84 and 2.98, respectively, in good agreement with those of Derouard and Lombardi.] Moreover, the effect of the energy defect diminishes very slowly with increasing n_0, roughly as n_0^{-1}.

The failure of both theories for $n_0<10$ reflects the quite different physical mechanisms at work in collisions with a target in a low-lying excited state, as opposed to one in a Rydberg state. Below $n_0=10$, the Na target is relatively opaque to He. The electron density of its excited (valence) electron is sufficiently large that first-order perturbation theory and the binary encounter approximation fails. Here an approach that models the transient complex formed by the system, such as expansion in quasimolecular electronic states [46], appears necessary.

Above $n_0=10$, however, the valence electron density becomes sufficiently Rydberg-like that perturbation theory and the binary encounter approximation succeed, the interaction of the Rydberg atom with the rare-gas projectile being such that a quasifree interaction model adequately describes the collision. In general, the onset of this high-n regime will depend on the nature of the Rydberg atom (its quantum defects and the importance of configuration interaction) and on the extent to which the internal structure of the projectile participates in the collision. Our study of l-mixing collisions of He with excited Na atoms confirms that for $n_0>10$ and absent significant configuration interaction, one may confidently model collisions of Rydberg species with He using the binary encounter approximation with a Fermi contact potential interaction and solving the scattering equations via first-order perturbation theory.

B. Alignment and oscillations in Ca–He collisions

Figure 2 shows quantum and semiclassical magnetic sublevel cross sections $\sigma^{|m_0|}(v)$ for the $17d\rightarrow 18p$ transition in Ca–He scattering. The results of the present calculations agree very well with those of the fully quantum-mechanical impulse approximation [27], even at relative velocities as low as several hundred m/s. Both theories predict significant alignment effects over the entire velocity range, the relative efficiency of a particular $|m_0|$ channel depending significantly on velocity. For these channels, σ^0 manifests the most pronounced oscillations, with peaks spaced as v^{-1}. The oscillations in σ^1 are equally evident, although their peaks are more widely spaced than those in σ^0. In sharp contrast, σ^2 shows no oscillations, varying smoothly with velocity; for large v, this variation conforms to the v^{-2} prediction of Eq. (19a).

Figure 3 deconstructs these magnetic sublevel cross sections into their state-to-state constituents. For clarity, these are separated into groups according to the initial magnetic quantum number $|m_0|$. Symmetry with respect to inversion through the origin and reflection through the azimuthal (xy) plane, imply, in the semiclassical theory, that cross sections for $m_0\rightarrow m$ and $m_0\rightarrow -m$ are equal. In the quantum theory, this symmetry is formally approximate; for this system, however, it holds to graphical accuracy [26,27]. In both theories, cross sections for $m_0\rightarrow m$ and for $-m_0\rightarrow -m$ are equal. Hence we show only non-negative values of m_0 and m. Figure 3 highlights the dependence of the oscillations in $\sigma^{|m_0|}$ on the initial quantum number $|m_0|$ and shows that for cases where $\sigma^{|m_0|}$ does oscillate, these structures arise from all contributing state-to-state cross sections. We further see that as v increases, the variation with velocity of all state-to-state cross sections reduces to the v^{-2} dependence expected from Eq. (19b).

The vital role of the energy defect $\Delta\epsilon$ for the oscillations is illustrated by the comparisons in Fig. 4 of magnetic sublevel cross sections from semiclassical calculations with $\Delta\epsilon=1.69\ \mathrm{cm}^{-1}$, the value for the $17d\rightarrow 18p$ transition in Ca, to those with $\Delta\epsilon=0$. (See Ref. [36] for an example of the significance of the energy defect for n, l-changing and quasielastic rare-gas atom Rydberg-atom collisions.) The zero-defect results manifest the familiar v^{-2} dependence at all velocities. The $\Delta\epsilon>0$ results, however, show this behavior

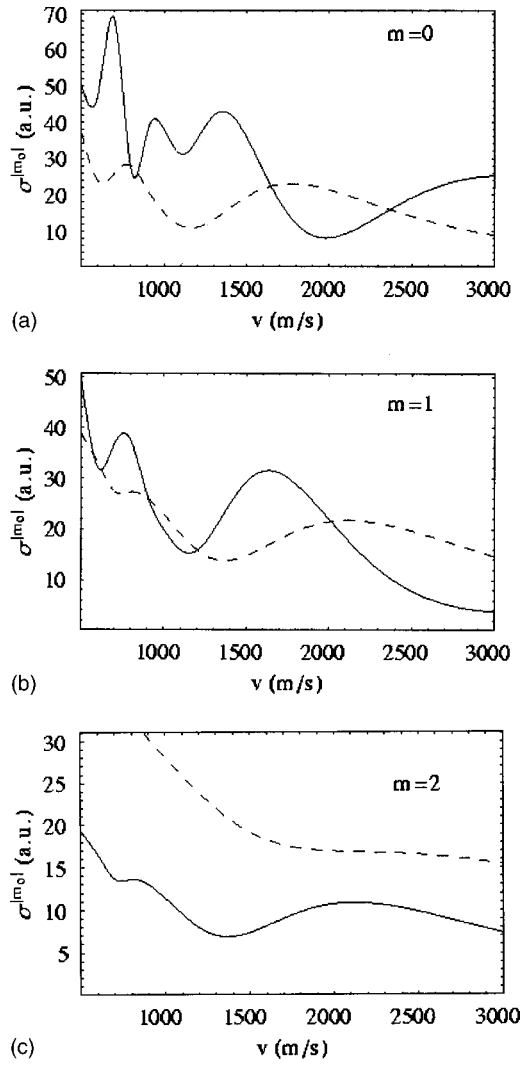

FIG. 3. State-to-state cross sections for $17d \rightarrow 18p$ transitions with various initial magnetic quantum numbers $|m_0|$: (upper) $0 \rightarrow 0$ and $0 \rightarrow 1$, (middle) $1 \rightarrow 0$ and $1 \rightarrow 1$, and (lower) $2 \rightarrow 0$ and $2 \rightarrow 1$. The solid lines corresponds to final magnetic quantum number $m=0$ and the dash lines to $m=1$.

only as $v \rightarrow \infty$, a limit that the cosine factor in Eq. (19b) shows to be equivalent to $\Delta\epsilon \rightarrow 0$.

Semiclassical and quantal calculations for the $23d \rightarrow 22f$ transition (not shown), for which the energy defect is 0.28 cm^{-1}, confirm this dependence on $\Delta\epsilon$. For this transition, none of the magnetic sublevel cross sections exhibit oscillations for $500 \leqslant v \leqslant 3000$ m/s. Alignment effects do, however, appear for $v \lesssim 1000$ m/s, where σ^2 exceeds σ^0 and σ^1, which are of comparable magnitude.

Almost as important as including the correct energy defect is properly accounting for the shift in phase of the radial function due to the core, $u_{nl}(r)$ of Eq. (8a). Many prior studies of rare-gas collisions with Rydberg atoms have approximated these functions by analytic hydrogenic forms. We have found this to be a very poor approximation for alignment effects in Ca-He cross sections.

In the Coulomb approximation [50], the potential energy of the Rydberg electron is replaced by the pure Coulomb

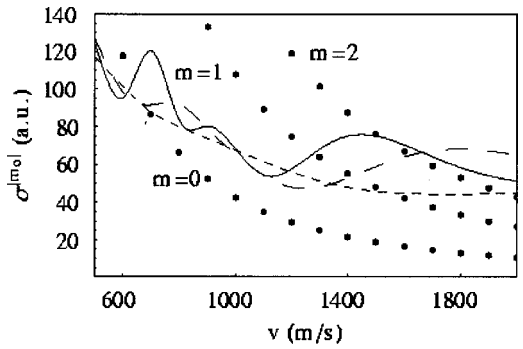

FIG. 4. Partial cross sections for $17d \rightarrow 18p$ transitions in Ca-He collisions calculated with energy defect $\Delta\epsilon = 1.69\ \mathrm{cm}^{-1}$ (curves) and in the zero-defect approximation (symbols) for $|m_0|=0$ (solid curve), 1 (long-dash curve), and 2 (short-dash curve).

potential $V(r) = Z_c/r$, where $Z_c = Z - N + 1$ with Z and N the nuclear charge and number of electrons, respectively. The radial Schrödinger equation is solved using the quantum-defect shifted energy of Eq. (7). Since this energy is not an eigenvalue of the pure-Coulomb Hamiltonian, radial functions that decay asymptotically ($r \rightarrow \infty$) blow up as $r \rightarrow 0$ unless they are cutoff at some radius r_c comparable to the size of the atom. We choose r_c to be the inner classical turning point. For a Rydberg state, the spatial extent of the radial function is so great that the region $0 < r < r_c$ is negligible. (For the states of Ca considered here, $r_c \approx 3a_0$, while the mean radii of these states is approximately $400a_0$.) Following Bates and Damgaard [49], we calculate radial functions from a truncated series approximation to the asymptotically decaying radial function. The most evident difference between the Bates–Damgaard radial functions and hydrogenic functions is a shift in their phase; we therefore refer to them as quantum-defect phase shifted radial functions.

Figure 5 compares magnetic sublevel cross sections calculated with these quantum-defect phase shifted radial functions [49] to values obtained using hydrogenic functions. The magnitudes of the hydrogenic cross sections are consistently below values obtained using phase shifted radial functions. And, although the hydrogenic cross sections do predict os-

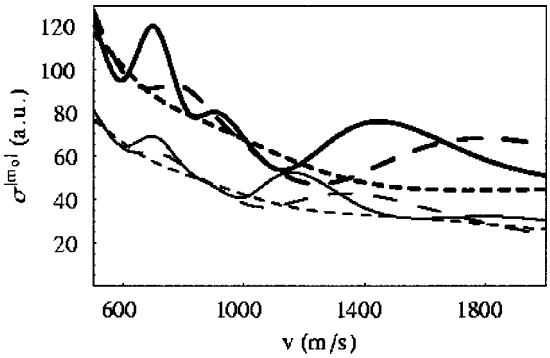

FIG. 5. Partial cross sections for $17d \rightarrow 18p$ transitions in Ca-He collisions calculated with quantum-defect phase-shifted radial functions (thick curves) and with hydrogenic radial function (thin curves) for $|m_0|=0$ (solid curves), 1 (long-dash curves), and 2 (short-dash curves).

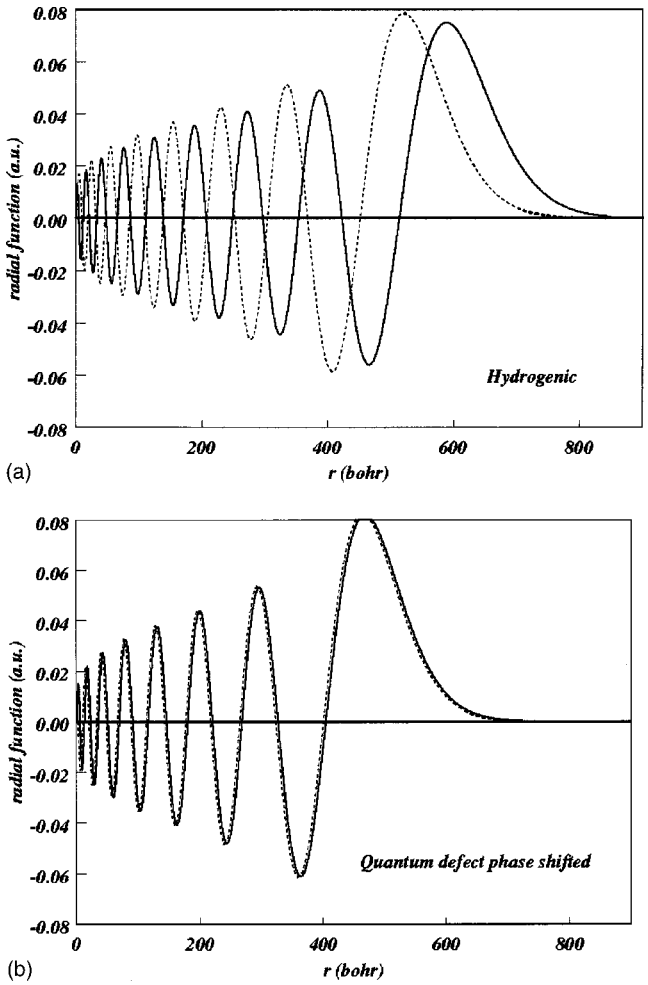

FIG. 6. Radial functions for the 17*d* (solid curves) and 18*p* (dash curves) states of Ca as calculated in the hydrogenic approximation (upper) and using the quantum defects of Ca (lower).

cillatory alignment effects, these predictions are qualitatively incorrect over much of the velocity range studied, in some cases incorrectly designating the order of these cross sections. For example, at about 1400 m/s, the cross section σ^0 calculated using hydrogenic functions lies between σ^1 and σ^2, whereas the more accurate σ^0 calculated with quantum-defect phase shifted functions clearly exceeds these two cross sections.

The reason for this sensitivity is evident from the comparison of hydrogenic and quantum-defect phase shifted radial functions in Fig. 6. The hydrogenic functions show a significant phase difference between the 17*d* and 18*p* states. This difference is all but eliminated when the quantum defects for these states are taken into account. Similar breakdowns in the hydrogenic approximation appear for other transitions [26].

V. INTERPRETATION

Equation (19b) explains the oscillations in the state-to-state and magnetic sublevel cross sections as interference phenomena resulting from the spatial distribution of Rydberg electron wave functions [28]. The functions in the radial

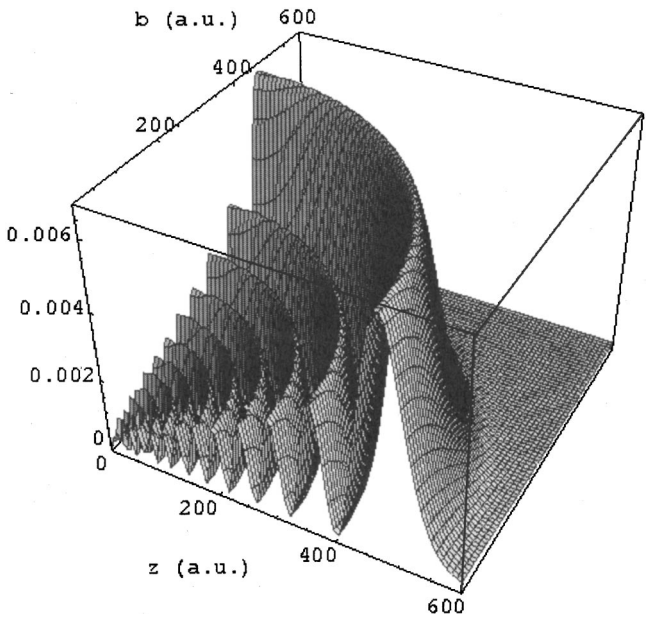

FIG. 7. Radial factors $u_{17d}(r)u_{18p}(r)$ in atomic units for r along the rare-gas atom trajectory.

product $u_{17d}(R)u_{18p}(R)$, which appears in the transition density factors in Eq. (19b), identify certain regions of space where Rydberg electron probabilities are higher than in adjacent regions. Figure 7 shows the resulting structure *in the radial product* for the $17d \rightarrow 18p$ transition densities along rare-gas atom trajectories $z(t)$ for contributing impact parameters b. For each transition $m_0 \rightarrow m$, this radial product is modulated by a different angular factor $P_2^{|m_0|}(\cos\theta)P_1^{|m|}(\cos\theta)$, where along a trajectory $\cos\theta = z/R$. For the $0 \rightarrow 0$ case, for example, the resulting transition density manifests the rich landscape of peaks and valleys seen in the density plots in part (a) of Fig. 8. An incident rare-gas atom finds several distinct regions along its trajectory where it can induce the transition $17d_0 \rightarrow 18p_0$.

The phase of the cosine function in Eq. (19b) is crucial to the probability that such a transition will actually occur. For fixed velocity v, the integrand in this equation will contribute significantly to the transition probability only for values of z and z' such that (a) the separation $z - z'$ is an integral multiple of the wavelength $2\pi\Delta\epsilon/\hbar v$, and (b) the transition density factors $\mathcal{P}_{\alpha'\alpha}(z,b)$ and $\mathcal{P}_{\alpha'\alpha}(z',b)$ are appreciable *at both z and z'*. One can understand the variation with v of the transition probability by (equivalently) varying the spacing $z - z'$ in the phase. As this spacing changes, the product $\mathcal{P}_{\alpha'\alpha}(z,b)\mathcal{P}_{\alpha'\alpha}(z',b)$ for the $0 \rightarrow 0$ transition in part (a) of Fig. 8 varies dramatically, as the points z and z' pass through peaks and valleys in the transition density. In effect, the factors $\mathcal{P}_{\alpha'\alpha}(z,b)$ and $\mathcal{P}_{\alpha'\alpha}(z',b)$ represent two ''opportunities'' or ''paths'' whereby the Rydberg electron can be excited to state α'. The cosine factor results in interference oscillations between these two excitation paths, i.e., between (acutely nonadiabatic) interactions at z and z'. It is not surprising, then, that these oscillations disappear as $\Delta\epsilon \rightarrow 0$, as in Fig. 4, or as $v \rightarrow \infty$, as in Fig. 3. Each state-to-state cross section, of course, entails an integral over impact parameter.

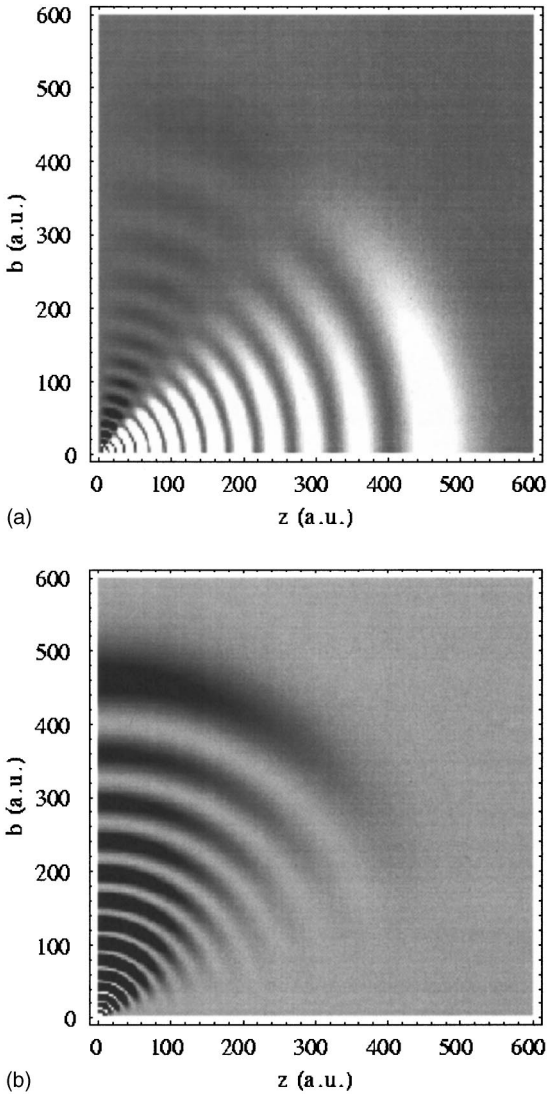

FIG. 8. Transition densities for the $0\rightarrow 0$ (upper figure) and $2\rightarrow 1$ (lower figure) state-to-state $17d_m\rightarrow 18p_{m'}$ transitions in Ca-He collisions. Light regions correspond to large values, dark to small values.

This integration complicates the picture but does not alter the qualitative predictions of Eq. (19b).

The different *angular* functions in the transition densities for different $m_0\rightarrow m$ transitions—the aforementioned products of associated Legendre polynomials—are responsible for the dependence of state-to-state and magnetic sublevel cross sections on magnetic quantum number. Consider the two extreme cases, $0\rightarrow 0$ and $2\rightarrow 1$. For $0\rightarrow 0$, the angular density $P_2^0 P_1^0$ is localized primarily along the z axis, parallel to the trajectory of the rare-gas atom. Together, the variation of the radial and angular products produces the rich array of regions of (comparatively) high transition probability in part (a) of Fig. 8, allowing plenty of opportunities for interference. By contrast, for $2\rightarrow 1$ the angular density $P_2^2 P_1^1$ is localized primarily in the xy plane. The resulting transition density for this case, shown in part (b) of Fig. 8, offers far less variation as the separation $z-z'$ (equivalently, the velocity) varies. The result is the smooth dependence with v of the $2\rightarrow 1$ cross section in Fig. 3.

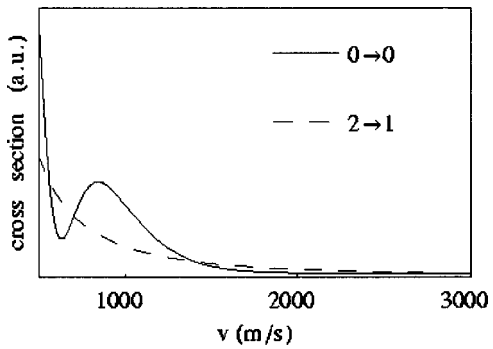

FIG. 9. Cross sections for a ''two-plane'' model of semiclassical $17d_m\rightarrow 18p_{m'}$ transitions in Ca-He collisions. For purposes of illustration, planes were located at $z_1=150a_0$ and $z_2=500a_0$.

To clarify further the origin of the oscillations, we consider the extreme model of a Rydberg state in which the electron presents to the rare-gas atom only two ''planes'' of transition density, one at z_1 and one at z_2, i.e., we approximate the transition density (13) by

$$\mathcal{P}_{\alpha'\alpha}[\mathbf{R}(t)]=\psi^*_{\alpha'}[\mathbf{R}(t)]\psi^*_{\alpha}[\mathbf{R}(t)]\{\delta[z(t)-z_1]+\delta[z(t)-z_2]\}. \tag{24}$$

Since in this model, transitions can occur only at interactions times t_1 or t_2, where $z(t_1)=z_1$ and $z(t_2)=z_2$, the transition probability (19b) reduces to

$$P_{\alpha_0\rightarrow\alpha}(v;b)=\left(\frac{2\pi A\hbar}{m_e}\right)^2\frac{1}{v^2}\left(\mathcal{P}^2_{\alpha'\alpha}(z_1,b)+\mathcal{P}^2_{\alpha'\alpha}(z_2,b)+2\cos\left[\frac{\Delta\epsilon}{\hbar v}(z_2-z_1)\right]\times\mathcal{P}_{\alpha'\alpha}(z_1,b)\mathcal{P}_{\alpha'\alpha}(z_2,b)\right). \tag{25}$$

All three appearances of the transition density $\mathcal{P}_{\alpha'\alpha}(z,b)$ in this result contribute to the dependence of the magnetic sublevel cross sections $\sigma^{|m_0|}(v)$ on initial magnetic quantum number $|m_0|$. But only the third term, a consequence of quantum-mechanical interference between excitation possibilities at planes at z_1 and z_2, can induce oscillations—and then only if the planes at z_1 and z_2 are at or near peaks in the two transition densities. Figure 9 shows the resulting cross sections *in this model* for the extreme cases $0\rightarrow 0$ and $2\rightarrow 1$ with planes at $z_1=150\,a_0$ and $z_2=500\,a_0$. These results are typical. Extensive tests (not shown) demonstrated that, provided z_1 and z_2 are far enough apart ($\Delta z\gtrsim 150a_0$), their particular values do not matter. One can easily find planes that induce oscillations in the $0\rightarrow 0$ cross section, while there are no planes that cause structure in the $2\rightarrow 1$ cross section. The variations in Fig. 3 with v and with m_0 and m of cross sections determined from the actual transition densities of Fig. 8 reflect the more distributed nature of these densities as compared with this two-plane model.

VI. CONCLUSION

The primary results of this study are three. First, our state-to-state cross sections calculated with quantum (impulse approximation) and semiclassical (rectilinear impact parameter, first-order perturbation) theories are in close agreement over most of the velocity range studied. Second, the semiclassical theory provides an interpretation of the oscillations in magnetic sublevel cross sections for Rydberg-atom-rare-gas collisions as due to quantum-mechanical path interference effects. And third, our study shows that previously used approximations—neglect the energy defect, and the hydrogenic approximation for Rydberg electron radial functions—are inappropriate for the study of alignment effects. The primary theoretical results are Eq. (19b), which reveals the origin of oscillations in these cross sections, and Eqs. (20), which greatly facilitates their calculation.

The cross sections in Figs. 2 and 3 show that despite quite different approaches to the dynamics, the quantal impulse and present semiclassical theories produce nearly identical magnetic sublevel and state-to-state cross sections for near-resonant energy transfer collisions of rare-gas atoms with Rydberg atoms. Only at the lowest relative velocities does this agreement break down. These two studies share only the Fermi contact potential, the spectator model of the core, and the representation of Rydberg electron radial functions by quantum-defect phase shifted radial functions. Implementation of both theories is of comparable (modest) difficulty, so the choice of theory can be based on the physical quantities of greatest interest. The present semiclassical approach highlights interpretation. If one seeks cross sections for collisions involving a rare-gas projectile that is more polarizable than He (e.g., Xe), then one may prefer the impulse approximation, where it is much easier to include the long-range electron-atom polarization interaction than in the present semiclassical treatment. For He, however, inclusion of polarization in no way alters the qualitative behavior of any of the cross sections presented here [26].

The importance of the energy defect illustrated in Fig. 4 implies that experiments to probe (or exploit) oscillations in $\sigma^{|m_0|}$ should emphasize transitions with the largest-energy defects, within the range of true Rydberg states and subject to experimental constraints. Although partial magnetic cross sections for lower-lying excited states manifest quite similar structures (as seen in the Ca-Xe calculations of Hickman [20]), the equations of the present theory are not directly applicable to transitions between such states.

The comparison in Fig. 5 between magnetic sublevel cross sections calculated with quantum-defect phase shifted radial functions and with hydrogenic functions argues strongly for the use of the former in future studies of rare-gas atom collisions with Rydberg atoms. While the method of Bates and Damgaard [49], which uses a truncated series approximation to the asymptotically decaying phase-shifted Coulomb function, works well for low-lying Rydberg states with small $\Delta l = l - l_0$, it encounters severe numerical difficulties for higher-n and/or larger Δl states.

The present calculations confirm the findings of recent experimental and quantal investigations that alignment effects do occur in near-resonant energy transfer collisions, even when the target state is a Rydberg atom. Both theoretical studies were designed to explicitly preclude the formation of a transient quasimolecular state during the collision. Instead, both treat the collision as a three-body process involving the Rydberg electron, the rare-gas atom, and the core of the Rydberg atom, whose role is reduced to that of a spectator. Both studies reveal identical oscillations, most pronounced in magnetic sublevel cross sections of low $|m_0|$, which depend strikingly on the relative velocity, the energy defect, and the initial magnetic quantum number.

In closing, we note that, while the measurements of Spain *et al.* corroborate the presence of alignment effects in near-resonant energy transfer cross sections for Rydberg atom-rare gas collisions, the predicted oscillations in these cross sections await confirmation or refutation by experiment. We hope the present findings will stimulate such experiments.

ACKNOWLEDGMENTS

We acknowledge useful conversations with Dr. J. Delos, Dr. N. F. Lane, Dr. A. P. Hickman, Dr. I. Fabrikant, Dr. G. A. Parker, Dr. K. Mullen, Dr. F. B. Dunning, Dr. J. P. Driessen, Dr. N. Shafer-Ray, and Dr. S. R. Leone and the support of the National Science Foundation under Grant No. PHY-9722055.

[1] M. O. Hale and S. R. Leone, J. Chem. Phys. **79**, 3352 (1983).
[2] M. O. Hale, I. V. Hertel, and S. R. Leone, Phys. Rev. Lett. **53**, 2296 (1984).
[3] W. Bussert, D. Neuschäfer, and S. R. Leone, J. Chem. Phys. **87**, 3833 (1987).
[4] L. J. Kovalenko, S. R. Leone, and J. B. Delos, J. Chem. Phys. **91**, 6948 (1989).
[5] R. L. Robinson, L. J. Kovalenko, and S. R. Leone, Phys. Rev. Lett. **64**, 388 (1990).
[6] R. L. Robinson, L. J. Kovalenko, C. J. Smith, and S. R. Leone, J. Chem. Phys. **92**, 5260 (1990).
[7] J. P. J. Driessen, C. J. Smith, and S. R. Leone, Phys. Rev. A **44**, R1431 (1991).
[8] J. P. J. Driessen, C. J. Smith, and S. R. Leone, J. Phys. Chem. **95**, 8163 (1991).
[9] J. P. J. Driessen and S. R. Leone, J. Phys. Chem. **96**, 6136 (1992).
[10] C. J. Smith, J. P. J. Driessen, L. Eno, and S. R. Leone, J. Chem. Phys. **96**, 8212 (1992).
[11] C. J. Smith, E. M. Spain, M. J. Dalberth, S. R. Leone, and J. P. J. Driessen, J. Chem. Soc., Faraday Trans. **89**, 1401 (1993).
[12] G. C. Schatz, L. J. Kovalenko, and S. R. Leone, J. Chem. Phys. **91**, 6961 (1989).
[13] B. J. Archer, N. F. Lane, and M. Kimura, Phys. Rev. A **42**, 6379 (1990).
[14] N. Andersen, J. W. Gallagher, and I. V. Hertel, Phys. Rep.

165, 1 (1988).
[15] N. Andersen, J. T. Broad, E. E. B. Campbell, J. W. Gallagher, and I. V. Hertel, Phys. Rep. **278**, 1 (1997).
[16] N. Andersen, K. Bartschat, J. T. Broad, and I. V. Hertel, Phys. Rep. **279**, 251 (1997).
[17] K. B. MacAdam and M. A. Morrison, Phys. Rev. A **48**, 1345 (1993).
[18] E. E. B. Campbell, H. Schmidt, and I. V. Hertel, Adv. Chem. Phys. **72**, 37 (1988).
[19] A. Berengolts, E. I. Dasevskaya, and E. E. Nikitin, J. Phys. B **26**, 3847 (1993).
[20] A. P. Hickman, J. J. Portman, S. Krebs, and W. Meyer, Phys. Rev. Lett. **72**, 1814 (1994).
[21] A. P. Hickman, Int. Rev. Phys. Chem. **16**, 177 (1997).
[22] A. P. Hickman, R. E. Olson, and J. Pascale, in *Rydberg States of Atoms and Molecules*, edited by R. F. Stebbings and F. B. Dunning (Cambridge University, Cambridge, 1983), Chap. 6, pp. 187–228.
[23] I. L. Beigman and V. S. Lebedev, Phys. Rep. **250**, 95 (1995).
[24] E. M. Spain, M. J. Dalberth, P. D. Kleiber, S. R. Leone, S. S. Op de Beek, and J. P. J. Driessen, J. Chem. Phys. **102**, 9522 (1995).
[25] E. M. Spain, M. J. Dalberth, P. D. Kleiber, S. R. Leone, S. S. Op de Beek, and J. P. J. Driessen, J. Chem. Phys. **102**, 9532 (1995).
[26] W. A. Isaacs, Ph.D. thesis, University of Oklahoma, 1996.
[27] W. A. Isaacs and M. A. Morrison, Phys. Rev. A **57**, R9 (1998).
[28] M. A. Morrison, E. G. Layton, and G. A. Parker, Phys. Rev. Lett. **84**, 1415 (2000).
[29] A. P. Hickman, Phys. Rev. A **18**, 1339 (1978).
[30] A. P. Hickman, Phys. Rev. A **19**, 994 (1979).
[31] A. P. Hickman, J. Phys. B **14**, L419 (1981).
[32] R. E. Olson, Phys. Rev. A **15**, 631 (1977).
[33] E. Fermi, Nuovo Cimento New Ser. **11**, 157 (1934).
[34] V. A. Alekseev and I. I. Sobel'man, Zh. Eksp. Teor. Fiz. **49**, 1274 (1965) [Sov. Phys. JETP **22**, 882 (1966)].
[35] M. R. C. McDowell and J. P. Coleman, *Introduction to the Theory of Ion-Atom Collisions* (Elsevier, New York, 1970).
[36] V. S. Lebedev and I. I. Fabrikant, Phys. Rev. A **54**, 2888 (1996).
[37] J. I. Gersten, Phys. Rev. A **14**, 1354 (1976).
[38] A. Omont, J. Phys. (Paris) **38**, 1343 (1977).
[39] J. Derouard and M. Lombardi, J. Phys. B **11**, 3875 (1978).
[40] E. de Prunelé and J. Pascale, J. Phys. B **12**, 2511 (1979).
[41] V. S. Lebedev and I. L. Beigman, *Physics of Highly Excited Atoms and Ions* (Springer-Verlag, New York, 1998).
[42] P. T. Greenland, Harwell Preprint TP 876, 1981.
[43] M. Karplus and R. N. Porter, *Atoms and Molecules* (Benjamin, Reading, MA, 1970).
[44] R. W. Crompton, M. T. Elford, and A. G. Robertson, Aust. J. Phys. **23**, 667 (1970).
[45] S. J. Buckman and B. Lohmann, J. Phys. B **19**, 2547 (1986).
[46] A. Kumar, N. F. Lane, and M. Kimura, Phys. Rev. A **39**, 1020 (1989).
[47] M. Kimura and N. F. Lane, Adv. At. Mol. Phys. **26**, 79 (1990).
[48] H. Friedrich, *Theoretical Atomic Physics*, 2nd ed. (Springer-Verlag, New York, 1998).
[49] D. R. Bates and A. Damgaard, Philos. Trans. R. Soc. London, Ser. A **242**, 101 (1949).
[50] C. Laughlin, Phys. Scr. **45**, 238 (1992).
[51] T. F. Gallagher, S. A. Edelstein, and R. M. Hill, Phys. Rev. Lett. **35**, 644 (1975).
[52] T. F. Gallagher, S. A. Edelstein, and R. M. Hill, Phys. Rev. A **15**, 1945 (1977).
[53] T. F. Gallagher, W. E. Cooke, and S. A. Edelstein, Phys. Rev. A **17**, 904 (1978).
[54] T. F. Gallagher, Phys. Rep. **210**, 319 (1992).
[55] T. F. Gallagher, *Rydberg Atoms* (Cambridge University, New York, 1994).
[56] A. A. Radzig and B. M. Smirnov, *Reference Data on Atoms, Molecules, and Ions* (Springer-Verlag, New York, 1980).
[57] L. Petitjean and F. Gounand, Phys. Rev. A **30**, 2946 (1984).
[58] V. S. Lebedev and I. I. Fabrikant, J. Phys. B **30**, 2649 (1997).
[59] V. S. Lebedev, J. Phys. B **31**, 1579 (1998).